Progress In Electromagnetics Research B, Vol. 49, 77–106, 2013

A THEORY OF MAGNETIC ANGLE SENSORS WITH HALL PLATES AND WITHOUT FLUXGUIDES

Udo Ausserlechner*

Infineon Technologies Austria AG, Siemensstrasse 2, Villach 9500, Austria

Abstract—Magnetic angle sensors detect the angular position of a permanent magnet attached to a rotating shaft. The magnet is polarized diametrically to the rotation axis. No soft magnetic flux guides are present. The semiconductor die is placed on and orthogonal to the rotation axis. There are two kinds of systems: (i) perpendicular systems detect the field components perpendicular to the rotation axis, and (ii) axial systems detect the component parallel to the rotation axis. The former use magneto-resistive sensors or vertical Hall effect devices; the latter use Hall plates. This paper focuses on axial systems, derives their conceptual limitations, and compares them with perpendicular systems. An optimized system and optimum shapes of magnets are reported. Angle errors due to assembly tolerances of magnet and sensor versus shaft are explained. It is proven that assembly tolerances of optimized axial systems give three times larger errors than perpendicular systems.

1. INTRODUCTION

This paper deals with angle sensors as shown in Fig. 1. A permanent magnet with diametrical magnetization is attached to the end of a rotating shaft whose angular position should be measured. A semiconductor die contains several magnetic field sensor elements. It is positioned orthogonal to the rotation axis with its center right on the rotation axis which is also a symmetry axis of the magnet. Along this axis the magnetic field is perpendicular to the axis and therefore parallel to the surface of the die. We call this class of sensors that respond to the magnetic field components perpendicular to the rotation axis *perpendicular angle sensors*. These can be magneto-resistors (MR) like, e.g., anisotropic magneto-resistors (AMR) [1] or

Received 10 January 2013, Accepted 5 February 2013, Scheduled 16 February 2013

* Corresponding author: Udo Ausserlechner (udo.ausserlechner@infineon.com).

giant magneto-resistors (GMR) [2–5] or tunnelling magneto-resistors (TMR). Alternatively one may also use vertical Hall effect devices (VHall) [6]. MRs respond to the angle between the in-plane component of the field and their in-plane reference direction, which is defined by layout or pre-magnetization during the manufacturing process. VHalls respond to a field component parallel to the die surface and orthogonal to the current streamlines through the device. With two such devices aligned in different directions one can infer both magnitude and angle of the in-plane field. All sensor technologies have their pros and cons: AMRs are accurate and stable, yet they are unambiguous only in a range of $0^\circ \ldots 180^\circ$. GMRs and TMRs cover the entire revolution $0^\circ \ldots 360^\circ$, yet they are less accurate and stable due to their pinned magnetization. All MRs need a minimum field strength (about 10 mT) for accurate operation. GMRs and TMRs also have a maximum allowed field (about 100 mT) to prevent minute drift of the pinned layer at high temperatures over lifetime. VHalls have no upper limit of destruction, are more robust, and their manufacturing costs are cheaper. Yet they suffer from larger noise [7] and larger residual offset [8] and also from crosstalk due to mechanical stress. Development of all these sensor technologies is ongoing and it is likely that the limits can be pushed significantly in the next decade.

Conversely, this paper focuses on *axial angle sensors*. They use the axial magnetic field component to infer the rotation angle. Since this component vanishes on the rotation axis one has to place the sensor devices off axis, e.g., on a circle of 1 mm diameter concentric to the axis (Section 3.2). As sensor elements one can use horizontal Hall plates (HHall) [9, 10] or MAGFETs [11]. The main advantage is the mature technology of HHalls, where the problems of offset [12] and mechanical stress [13, 14] are solved. Another advantage is the differential sensing principle, which is robust against background magnetic fields. However, this works only if the Hall plates match well despite mechanical stress gradients (Appendix E).

Which is the optimum angle sensor? A simple answer focuses on the sensor elements, yet there differences diminish: of course VHalls have more noise than MRs, yet for moderate speed this is irrelevant. Hall devices have no hysteresis, yet this becomes irrelevant if MR-technology pushes hysteresis limits below 0.05°. Limitations like 180°-ambiguity of AMRs or mechanical stress on Hall devices can be tackled by additional circuitry. In practice it turns out that a major part of the angle error is caused by assembly tolerances. So a more prospective answer on optimum sensors accounts for these tolerances. This error can be limited by optimum layout and shape of magnets. Yet even then a residual error remains due to misalignments. Are these limitations

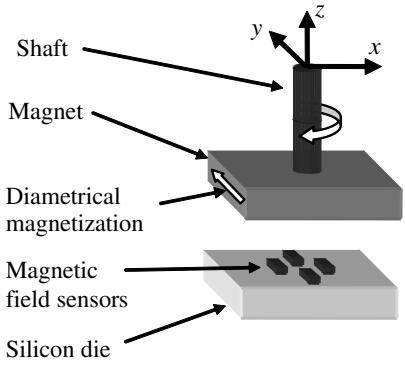

Figure 1. Angle sensor composed of a diametrically polarized magnet attached to the end of a rotating shaft and a sensor die placed on the rotation axis. In the case of axial angle sensors the magnetic field sensor elements respond to the z-component of the field. For perpendicular angle sensors the magnetic field sensor elements respond to the x-and y-components of the field.

identical for all systems or are there some preferable over others? Indeed, the following discussion shows that axial angle sensors have considerably larger errors than perpendicular ones.

2. THE PRINCIPLE OF AXIAL ANGLE SENSORS

Figure 2 shows the axial field component of a diametrically polarized magnet. Although the function has a complex shape for radial distances near the perimeter, it is well behaved near the rotation axis: there it is an odd function in y, proportional to y-position, and independent of x-position

$$B_z(x,y) = Cy + O\left(y^3\right), \quad C \approx 33\,\mathrm{mT/mm} \text{ for } 0.5\,\mathrm{mm} \text{ air-gap} \tag{1}$$

When the magnet rotates by an angle φ also this plane rotates

$$B_z(x,y) = C(x\sin\varphi + y\cos\varphi) + O\left((x\sin\varphi + y\cos\varphi)^3\right). \tag{2}$$

Obviously one may sample the plane by an array of Hall plates distributed over the silicon die. Then it is straightforward to infer the rotation angle. Apparently the array of Hall plates must not extend too far off the axis, because there the field deviates from the plane and this leads to errors in the estimated angle. On the other hand the sensor elements must not be too close to the axis, because then the field is too small. Therefore the array of Hall plates is usually located within an area of $2\,\mathrm{mm} \times 2\,\mathrm{mm}$ around the rotation axis.

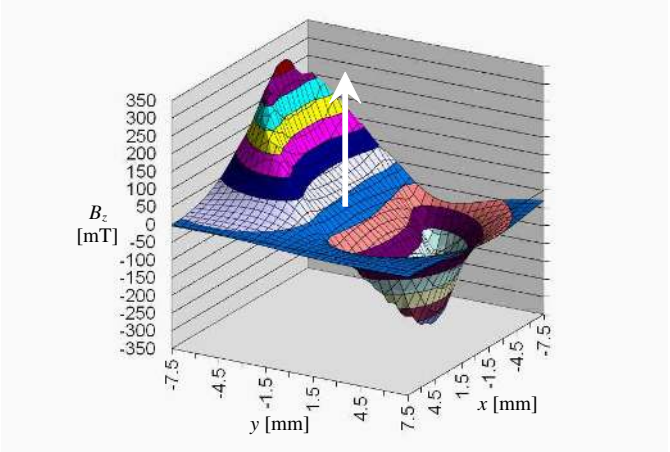

Figure 2. Axial field component of a nickel coated cylindrical NdFeB magnet with 10 mm diameter and 4 mm thickness, magnetized along y-axis. The field is measured 0.5 mm above the top surface of the magnet. The rotation axis is shown as an arrow. Near the center the function is close to a plane that is parallel to the x-axis.

As for the shape of the array of Hall plates there are numerous possibilities. In principle three Hall plates are enough to reconstruct the plane equation. As all rotation angles should be detected with the same sensitivity the Hall plates should be evenly distributed. This leads to three Hall plates along a circle of diameter $2R_0$, concentric to the rotation axis. The Hall plates are located at angles 0°, 120°, and 240°. However, the Hall plates have a finite size of around 100 µm × 100 µm and therefore it would be necessary to rotate their shapes around the origin, too. In some CMOS processes this is incompatible to basic layout rules: devices must be aligned along the x- or y-axis. This calls for a system having four square Hall plates positioned at the locations $(x_1, y_1) = (R_0, 0)$, $(x_2, y_2) = (0, R_0)$, $(x_3, y_3) = (-R_0, 0)$, $(x_4, y_4) = (0, -R_0)$, where the subscripts label the Hall plate. We call it an axialC4 system (angle sensor responsive to the *axial* field component, C4: with 4 sensor elements on a circle). In the absence of assembly tolerances the output signals of the Hall plates are

$$\begin{aligned} h_1 &= B_z(R_0, 0, \varepsilon_z), \quad h_2 = B_z(0, R_0, \varepsilon_z), \\ h_3 &= B_z(-R_0, 0, \varepsilon_z), \quad h_4 = B_z(0, -R_0, \varepsilon_z) \end{aligned} \tag{3}$$

where ε_z is the axial distance of the Hall plates to the center of the magnet. Thereby we assume that Hall plates respond only to z-components of the magnetic field (cf. Appendix B for a more accurate

nonlinear model). Since $h_1 = -h_3$ and $h_2 = -h_4$ we get

$$h_{13} = h_1 - h_3, \quad h_{24} = h_2 - h_4. \tag{4}$$

Equations (2) and (4) give

$$h_{13} = 2CR_0 \sin\varphi + O\left(\sin^3\varphi\right), \quad h_{24} = 2CR_0 \cos\varphi + O\left(\cos^3\varphi\right). \tag{5}$$

Thus h_{13} and h_{24} are in quadrature and so one can compute the angle φ (e.g., by the CORDIC algorithm). So the principle is straightforward, but how about the error terms $O\left(\sin^3\varphi\right)$ and $O\left(\cos^3\varphi\right)$?

3. MAGNETS FOR AXIAL ANGLE SENSORS

3.1. Symmetry Property of Useful Magnets

The symmetry properties $h_1 = -h_3$ and $h_2 = -h_4$ require

$$B_z(-x, -y, z) = -B_z(x, y, z). \tag{6}$$

The field of a magnet with homogeneous magnetization $\vec{M}$ is given as a surface integral in (A.1) in [4] (where primed coordinates denote the source points and unprimed the test point):

$$B_z(x, y, z) = \frac{\mu_0}{4\pi} \oint_A \frac{z - z'}{\left((x-x')^2 + (y-y')^2 + (z-z')^2\right)^{3/2}} \left(\vec{M} \cdot d\vec{A'}\right) \tag{7}$$

Thus one may write for $B_z(-x, -y, z)$

$$\frac{\mu_0}{4\pi} \oint_A \frac{(z - z')\, M_n\left(x', y', z'\right)}{\left((x + x')^2 + (y + y')^2 + (z - z')^2\right)^{3/2}} dA' \tag{8}$$

where $M_n(x', y', z')$ is the component of the magnetization normal to the surface of the magnet and pointing outwards. With

$$M_n\left(-x', -y', z'\right) = -M_n\left(x', y', z'\right) \tag{9}$$

Equation (8) becomes

$$\frac{\mu_0}{4\pi} \oint_A \frac{(z - z')\,(-1)\, M_n\left(-x', -y', z'\right)}{\left((x + x')^2 + (y + y')^2 + (z - z')^2\right)^{3/2}} dA' \tag{10}$$

and with $-x' = x''$, $-y' = y''$, $z' = z''$ one may write for (8)

$$-\frac{\mu_0}{4\pi} \oint_A \frac{(z - z'')\, M_n\left(x'', y'', z''\right)}{\left((x - x'')^2 + (y - y'')^2 + (z - z'')^2\right)^{3/2}} dA'' = -B_z(x, y, z). \tag{11}$$

Thus, magnets with the mirror symmetry (9) fulfill (6). All magnets with rotational shape belong to this group, but also block-shaped magnets do — even more general shapes are thinkable.

So (9) is a necessary requirement, but is it also sufficient for a good sensor? This is discussed in the next subsection.

3.2. Rotational Symmetry of Useful Magnets

Consider a magnet of rotational geometry with homogeneous magnetization in y-direction. In the general case (e.g., a cone) the radius R' is a function of z'. In cylindrical coordinates one gets

$$B_x(R,\psi,z) = \mu_0 M \sin(2\psi)\, b_1 \tag{12a}$$

$$B_y(R,\psi,z) = \mu_0 M \{b_0 - \cos(2\psi)\, b_1\} \tag{12b}$$

$$B_z(R,\psi,z) = \mu_0 M \sin\psi b_2 \tag{12c}$$

$$b_0 = \frac{1}{16} \int_{z'=-H/2}^{H/2} R' \frac{3RkF_2\left(k^2\right) - 4R'F_1\left(k^2\right)}{\left(R^2 + R'^2 + (z-z')^2\right)^{3/2}} dz' \tag{12d}$$

$$b_1 = \frac{R}{8} \int_{z'=-H/2}^{H/2} R'^2 \frac{3RF_2\left(k^2\right) - (15/8)\, R'kF_3\left(k^2\right)}{\left(R^2 + R'^2 + (z-z')^2\right)^{5/2}} dz' \tag{12e}$$

$$b_2 = \frac{3R}{4} \int_{z'=-H/2}^{H/2} \frac{(z-z')R'^2F_2\left(k^2\right)}{\left(R^2 + R'^2 + (z-z')^2\right)^{5/2}} dz' \tag{12f}$$

with $k = 2RR'/(R^2 + R'^2 + (z-z')^2)$ and H being the thickness of the magnet. Hereby (12c) was derived from (7), (12a) and (12b) are obtained in an analogous way from (A.1) in [4]. Although these integrals (12d), (12e), (12f) are complicated expressions containing hypergeometric functions $F_n(k^2) = {}_2F_1(n/2 + 1/4,\, n/2 + 3/4,\, n,\, k^2)$ they bring new insight: The field B_z is sinusoidal versus ψ — no higher harmonics are involved. With (4) and (12c) the signals are

$$h_{13} = 2\mu_0 M b_2 \sin\varphi, \quad h_{24} = 2\mu_0 M b_2 \cos\varphi, \tag{13}$$

φ is the rotation angle whereas ψ is the azimuthal coordinate of the test point. Therefore homogeneously magnetized samples of rotational symmetry are perfectly suited for axial angle sensors.

Does that mean that magnets of other than rotational symmetry are not apt for axial angle sensors? As an example we have a look on parallel epipeds of size $2a \times 2\underline{b} \times 2c$, magnetized in y-direction (denoted by the underline). According to [15] the axial field is

$$B_z(R,\psi,z) = \frac{\mu_0 M}{4\pi} \sum_{l,m,n=1}^{2} (-1)^{l+m+n} \ln\Bigg(R\cos\psi + (-1)^l a + \sqrt{\begin{array}{l}\left(R\cos\psi + (-1)^l a\right)^2 \\ + \left(R\sin\psi + (-1)^m b\right)^2 + \left(z + (-1)^n c\right)^2\end{array}}\Bigg) \tag{14}$$

For small R (14) can be developed into a Taylor series, but obviously this series expansion contains higher harmonics in ψ. This shows that block shaped magnets are not well suited for axial angle sensors. They lead to angle errors even with perfectly accurate assembly and with perfect Hall plates and signal conditioning circuit. Of course these errors get smaller for large magnets $R \ll a, b$. Fig. 3 shows an example for a magnet of size 6 mm × 6 mm × 3 mm and angle sensors located on a Hall circle with 1.1 mm diameter, 1 mm below the magnet. Obviously the axialC4 system has a significant error of 0.7° with 90° periodicity. Fig. 4 shows an axialC8 system that is composed of two axialC4 sub-systems rotated by 45° against each other. Each sub-system estimates the rotation angle. The errors of each subsystem are like for the axialC4 system, also rotated by 45° against each other. Thus, if the estimated angles of both sub-systems are averaged, their errors cancel (due to the 90° periodicity) and only a minute error is left (less than 0.005°). The conclusion is that an axialC4 system leads to significant errors for block-shaped magnets, yet these errors can be cancelled by an axialC8 system. However, the price is to double the computing power. The system has to compute two angles of axialC4 sub-systems. This might be done sequentially, yet it costs speed.

In practice, even magnets of rotational symmetry produce higher harmonics so that (13) does not hold accurately. One reason is lack of homogeneity of magnetization. Good homogeneity requires slim magnets (i.e., large ratio of diameter over thickness). Other reasons

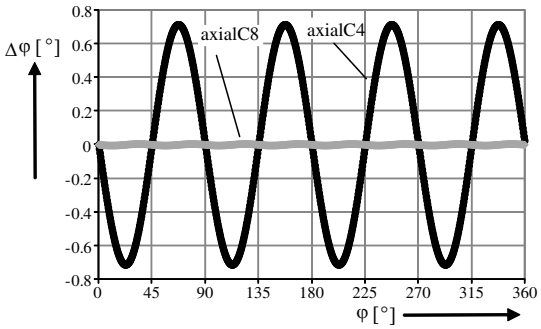

Figure 3. Theoretical angle errors $\Delta\varphi$ of axial angle sensors with a block-shaped magnet 6 mm × 6 mm × 3 mm. The Hall plates are located on a circle with 1.1 mm diameter, 1 mm below the bottom surface of the magnet. The axialC4 system has a significant error of 0.7° with a $\sin(4\varphi)$ dependency. An axialC8 system has a greatly improved error with a $\sin(8\varphi)$ dependency.

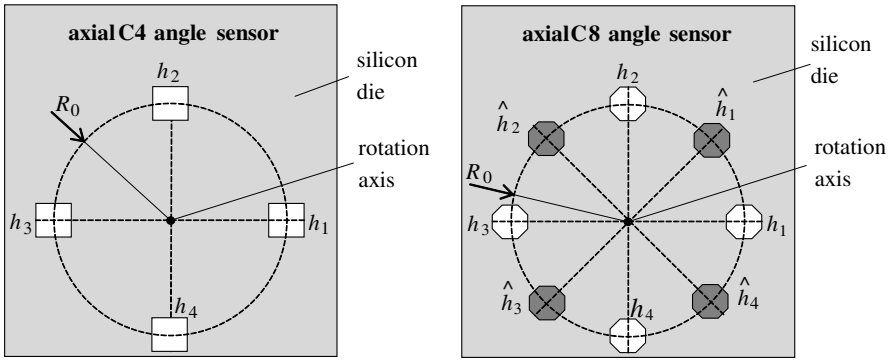

Figure 4. Layouts of axial angle sensors. The axialC4 angle sensor is composed of four Hall plates evenly spaced at a Hall circle with radius R_0 around the rotation axis. The axialC8 angle sensor consists of two axialC4 cells rotated 45° against each other. The output of the axialC8 angle sensor is the average of the outputs of both axialC4 cells. The axialC8 angle sensor is more accurate and works with more general shapes of magnets than the axialC4 angle sensor.

may be anisotropic sinter shrinkage of the magnet or soft magnetic coating of rear earth magnets. In order not to pose too stringent requirements on the magnet one has to use axialC8 instead of axialC4 systems. An alternative system with similar performance like axialC8 systems is sketched in Appendix D.

Applying Maxwell's equations to (12) gives several relations between derivatives, which will be used in the sequel to simplify the angle error. From curl $\vec{B} = 0$ one gets $\partial B_x/\partial y = \partial B_y/\partial x$, $\partial B_y/\partial z = \partial B_z/\partial y$, $\partial B_x/\partial z = \partial B_z/\partial x$. With $R^2 = x^2 + y^2$ and $\tan\psi = y/x$ one gets $\partial/\partial x = \cos\psi\partial/\partial R - (\sin\psi/R)\partial/\partial\psi$ and $\partial/\partial y = \sin\psi\partial/\partial R + (\cos\psi/R)\partial/\partial\psi$ in cylindrical coordinates (R, ψ, z). This gives

$$\frac{\partial b_1}{\partial R} + 2\frac{b_1}{R} = \frac{\partial b_0}{\partial R},\ \frac{\partial b_2}{\partial R} - \frac{b_2}{R} = 2\frac{\partial b_1}{\partial z},\ \frac{\partial b_2}{\partial R} + \frac{b_2}{R} = 2\frac{\partial b_0}{\partial z}. \tag{15}$$

From div $\vec{B} = 0$ one gets

$$2\frac{\partial b_0}{\partial R} + \frac{\partial b_2}{\partial z} = 0. \tag{16}$$

Furthermore, each of the components $B_x,\ B_y,\ B_z$ fulfills the Laplace equation. This gives

$$\frac{\partial^2 b_0}{\partial R^2} + \frac{1}{R}\frac{\partial b_0}{\partial R} + \frac{\partial^2 b_0}{\partial z^2} = 0 \tag{17a}$$

$$\frac{\partial^2 b_1}{\partial R^2} + \frac{1}{R}\frac{\partial b_1}{\partial R} + \frac{\partial^2 b_1}{\partial z^2} = 4\frac{b_1}{R^2} \tag{17b}$$

$$\frac{\partial^2 b_2}{\partial R^2} + \frac{1}{R}\frac{\partial b_2}{\partial R} + \frac{\partial^2 b_2}{\partial z^2} = \frac{b_2}{R^2} \tag{17c}$$

4. ERRORS DUE TO ASSEMBLY TOLERANCES

4.1. How Assembly Tolerances Affect the Magnetic Field

A reference frame (x, y, z) is fixed to the rotating magnet, and another reference frame $\left(x^{(8)}, y^{(8)}, z^{(8)}\right)$ is fixed to the sensor die. The Hall plates are assumed to be point sized. The first Hall plate is located at $\left(x^{(8)}, y^{(8)}, z^{(8)}\right) = (R_0, 0, 0)$, the second one at $\left(x^{(8)}, y^{(8)}, z^{(8)}\right) = (0, R_0, 0)$, the third one at $\left(x^{(8)}, y^{(8)}, z^{(8)}\right) = (-R_0, 0, 0)$, and the fourth one at $\left(x^{(8)}, y^{(8)}, z^{(8)}\right) = (0, -R_0, 0)$. Since all Hall plates are on the surface of the die $z^{(8)} = 0$ holds for all of them (Errors due to chip warpage are discussed in Appendix C). The coordinate transformation between the two reference frames (x, y, z) and $\left(x^{(8)}, y^{(8)}, z^{(8)}\right)$ is given in [1, 4, 5]: it is a lengthy function of the rotation angle and the assembly tolerances. All relevant assembly tolerances are listed in Table 1. They are also identical to preceding works [1, 4, 5].

Table 1. Assembly tolerances.

Symbol	Description
$\delta_x = \delta_r \cos\eta$, $\delta_y = \delta_r \sin\eta$	Eccentricity of the magnet with respect to the axis of rotation
δ_z	Shift of magnet along the axis of rotation
$\varepsilon_x = \varepsilon_r \cos\chi$, $\varepsilon_y = \varepsilon_r \sin\chi$	Eccentricity of sensor die with respect to the axis of rotation
ε_z	Distance of Hall plates to center of magnet
α	Angle between magnetization and tilt axis of magnet
β	Tilt of magnet against axis of rotation
φ	Angle of rotation of the shaft
γ	Angle between x-axis on sensor die and tilt axis of sensor die
λ	Tilt of die against axis of rotation
ϑ	Azimuthal twist angle of sensor die in its own surface

Thus we can express the vertical magnetic flux density on the surface of the die

$$\begin{aligned}
B_z^{(8)}\left(x^{(8)},y^{(8)},0\right) &= (\cos\beta\cos\lambda-\cos\gamma\cos\varphi\sin\beta\sin\lambda\\
&+\sin\beta\sin\gamma\sin\lambda\sin\varphi)B_z(x,y,z)\\
&+(\cos\alpha\cos\lambda\sin\beta-(\cos\varphi\sin\alpha+\cos\alpha\cos\beta\sin\varphi)\sin\gamma\sin\lambda\\
&+(\cos\alpha\cos\beta\cos\varphi-\sin\alpha\sin\varphi)\cos\gamma\sin\lambda)\,B_x\,(x,y,z)\\
&+(\sin\alpha\cos\lambda\sin\beta+(\sin\varphi\cos\alpha+\sin\alpha\cos\beta\cos\varphi)\cos\gamma\sin\lambda\\
&+(-\sin\alpha\cos\beta\sin\varphi+\cos\alpha\cos\varphi)\sin\gamma\sin\lambda)\,B_y\,(x,y,z) \qquad (18a)
\end{aligned}$$

with

$$\begin{aligned}
x &= \delta_x+\cos\alpha\sin\beta\left(\varepsilon_z-R^{(8)}\sin\lambda\cos\left(\vartheta+\psi^{(8)}\right)\right)\\
&+(\cos\alpha\cos\beta\cos\varphi-\sin\alpha\sin\varphi)\left(\varepsilon_x+R^{(8)}\cos\gamma\cos\lambda\cos\left(\vartheta+\psi^{(8)}\right)\right.\\
&\left.-R^{(8)}\sin\gamma\sin\left(\vartheta+\psi^{(8)}\right)\right)\\
&-(\cos\varphi\sin\alpha+\cos\alpha\cos\beta\sin\varphi)\left(\varepsilon_y+R^{(8)}\sin\gamma\cos\lambda\cos\left(\vartheta+\psi^{(8)}\right)\right.\\
&\left.+R^{(8)}\cos\gamma\sin\left(\vartheta+\psi^{(8)}\right)\right) \qquad (18b)\\
y &= \delta_y+\sin\alpha\sin\beta\left(\varepsilon_z-R^{(8)}\sin\lambda\cos\left(\vartheta+\psi^{(8)}\right)\right)\\
&+(\sin\alpha\cos\beta\cos\varphi+\cos\alpha\sin\varphi)\left(\varepsilon_x+R^{(8)}\cos\gamma\cos\lambda\cos\left(\vartheta+\psi^{(8)}\right)\right.\\
&\left.-R^{(8)}\sin\gamma\sin\left(\vartheta+\psi^{(8)}\right)\right)\\
&+(\cos\varphi\cos\alpha-\sin\alpha\cos\beta\sin\varphi)\left(\varepsilon_y+R^{(8)}\sin\gamma\cos\lambda\cos\left(\vartheta+\psi^{(8)}\right)\right.\\
&\left.+R^{(8)}\cos\gamma\sin\left(\vartheta+\psi^{(8)}\right)\right) \qquad (18c)\\
z &= \delta_z+\cos\beta\left(\varepsilon_z-R^{(8)}\sin\lambda\cos\left(\vartheta+\psi^{(8)}\right)\right)\\
&+R^{(8)}\sin\beta\sin(\gamma+\varphi)\sin\left(\vartheta+\psi^{(8)}\right)\\
&-\sin\beta\cos\varphi\left(\varepsilon_x+R^{(8)}\cos\gamma\cos\lambda\cos\left(\vartheta+\psi^{(8)}\right)\right)\\
&+\sin\beta\sin\varphi\left(\varepsilon_y+R^{(8)}\sin\gamma\cos\lambda\cos\left(\vartheta+\psi^{(8)}\right)\right) \qquad (18d)
\end{aligned}$$

where we used $x^{(8)}=R^{(8)}\cos\psi^{(8)}$, $y^{(8)}=R^{(8)}\sin\psi^{(8)}$. All Hall plates are at $R^{(8)}=R_0$ and $\psi^{(8)}=0,\pi/2,\pi,3\pi/2$, respectively. If assembly tilts β, λ, twist ϑ, and eccentricities δ_x, δ_y, ε_x, ε_y vanish (18a)

simplifies to

$$B_z^{(8)}\left(x^{(8)}, y^{(8)}, 0\right) = B_z\left(R_0\cos\left(\alpha+\gamma+\varphi+\psi^{(8)}\right), R_0\sin\left(\alpha+\gamma+\varphi+\psi^{(8)}\right), \delta_z+\varepsilon_z\right). \quad (19)$$

For magnets with rotational symmetry this gives

$$h_{13} = 2\mu_0 M b_2 \sin(\alpha+\gamma+\varphi), \quad h_{24} = 2\mu_0 M b_2 \cos(\alpha+\gamma+\varphi) \quad (20)$$

with $b_2 = b_2(R_0, \delta_z+\varepsilon_z)$. So the system estimates the rotation angle by

$$\varphi' = \arctan(h_{13}/h_{24}) - \alpha - \gamma. \quad (21)$$

With assembly tolerances the true rotation angle φ and the estimated angle φ' differ by the error $\Delta\varphi = \varphi - \varphi'$. Thus, (21) gives

$$\tan\Delta\varphi = \frac{h_{24}\sin(\alpha+\gamma+\varphi) - h_{13}\cos(\alpha+\gamma+\varphi)}{h_{24}\cos(\alpha+\gamma+\varphi) + h_{13}\sin(\alpha+\gamma+\varphi)}. \quad (22)$$

This holds for arbitrary magnets and arbitrary radius R of the Hall circle.

4.2. Errors of AxialC4 Sensors due to Assembly Tolerances

In (22) the signals h_{13} and h_{24} are lengthy functions of rotation angle, assembly tolerances, and magnet according to (4) and (18). The expressions get shorter if we approximate them by a Taylor series like in [1, 4, 5], which is admissible for small assembly tolerances. A convenient way to do this with an algebraic computer program like MATHEMATICA is to multiply all small quantities $\beta, \lambda, \vartheta, \delta_x, \delta_y, \varepsilon_x, \varepsilon_y$ in (18) by a parameter s, and let the program do the series expansion in $s = 0$ up to second order of s. Thereby the coordinates of the test point depend on the assembly tolerances. So they are functions of s: $R \to R(s)$, $\psi \to \psi(s)$, $z \to z(s)$. Therefore derivatives of coordinates with respect to s show up in the series

$$\begin{aligned}
B_z^{(8)} &= B_z \\
&+s\{B_x(\beta\cos\alpha+\lambda\cos(\alpha+\gamma+\varphi))+B_y(\beta\sin\alpha+\lambda\sin(\alpha+\gamma+\varphi)) \\
&+z'\frac{\partial B_z}{\partial z}+\psi'\frac{\partial B_z}{\partial\psi}+R'\frac{\partial B_z}{\partial R}\Big\}+s^2\left\{\frac{-\beta^2-\lambda^2-2\beta\lambda\cos(\gamma+\varphi)}{2}B_z\right. \\
&+\frac{z''}{2}\frac{\partial B_z}{\partial z}+\frac{(z')^2}{2}\frac{\partial^2 B_z}{\partial z^2}+\frac{\psi''}{2}\frac{\partial B_z}{\partial\psi}+\psi' z'\frac{\partial^2 B_z}{\partial\psi\partial z} \\
&+\frac{(\psi')^2}{2}\frac{\partial^2 B_z}{\partial\psi^2}+\frac{R''}{2}\frac{\partial B_z}{\partial R}+R' z'\frac{\partial^2 B_z}{\partial R\partial z}+R'\psi'\frac{\partial^2 B_z}{\partial R\partial\psi}+\frac{(R')^2}{2}\frac{\partial^2 B_z}{\partial R^2}
\end{aligned}$$

$$+(\beta\cos\alpha+\lambda\cos(\alpha+\gamma+\varphi))\left(R'\frac{\partial B_x}{\partial R}+\psi'\frac{\partial B_x}{\partial\psi}+z'\frac{\partial B_x}{\partial z}\right)$$
$$+(\beta\sin\alpha+\lambda\sin(\alpha+\gamma+\varphi))\left(R'\frac{\partial B_y}{\partial R}+\psi'\frac{\partial B_y}{\partial\psi}+z'\frac{\partial B_y}{\partial z}\right)\Bigg\}+O\left(s^3\right) \quad (23)$$

with B_x, B_y, B_z evaluated at $R(0)=R_0$, $\psi(0)=\alpha+\gamma+\varphi+\psi^{(8)}$, and $z(0)=\varepsilon_z+\delta_z$. The first derivatives are

$$R' = \frac{dR(0)}{ds}=\varepsilon_r\cos\left(\chi-\gamma-\psi^{(8)}\right)+\delta_r\cos\left(\alpha-\eta+\gamma+\varphi+\psi^{(8)}\right)$$
$$+\beta\varepsilon_z\cos\left(\gamma+\varphi+\psi^{(8)}\right) \quad (24a)$$

$$\psi' = \frac{d\psi(0)}{ds}=\vartheta+\frac{\varepsilon_r}{R_0}\sin\left(\chi-\gamma-\psi^{(8)}\right)$$
$$-\frac{\delta_r}{R_0}\sin\left(\alpha-\eta+\gamma+\varphi+\psi^{(8)}\right)-\beta\frac{\varepsilon_z}{R_0}\sin\left(\gamma+\varphi+\psi^{(8)}\right) \quad (24b)$$

$$z' = \frac{dz(0)}{ds}=-\lambda R_0\cos\psi^{(8)}-\beta R_0\cos\left(\gamma+\varphi+\psi^{(8)}\right) \quad (24c)$$

The second derivatives are

$$R'' = \frac{d^2R(0)}{ds^2}=\frac{\delta_r^2}{2R_0}+\frac{\varepsilon_r^2}{2R_0}+\frac{\beta^2\varepsilon_z^2}{2R_0}-\left(\beta^2+\lambda^2\right)\frac{R_0}{2}+\beta\frac{\delta_r\varepsilon_z}{R_0}\cos(\alpha-\eta)$$
$$+\beta\frac{\varepsilon_r\varepsilon_z}{R_0}\cos(\chi+\varphi)+\frac{\delta_r\varepsilon_r}{R_0}\cos(\alpha+\chi-\eta+\varphi)-\beta\lambda R_0(\cos(\gamma+\varphi)$$
$$+\cos\left(\gamma+\varphi+2\psi^{(8)}\right))-\lambda^2\frac{R_0}{2}\cos\left(2\psi^{(8)}\right)-\frac{\varepsilon_r^2}{2R_0}\cos\left(2\left(\chi-\gamma-\psi^{(8)}\right)\right)$$
$$-\beta\frac{\varepsilon_r\varepsilon_z}{R_0}\cos\left(\chi-2\gamma-\varphi-2\psi^{(8)}\right)-\beta^2\frac{\varepsilon_z^2}{2R_0}\cos\left(2\left(\gamma+\varphi+\psi^{(8)}\right)\right)$$
$$-\beta^2\frac{R_0}{2}\cos\left(2\left(\gamma+\varphi+\psi^{(8)}\right)\right)-\frac{\delta_r^2}{2R_0}\cos\left(2\left(\alpha-\eta+\gamma+\varphi+\psi^{(8)}\right)\right)$$
$$+2\varepsilon_r\vartheta\sin\left(\chi-\gamma-\psi^{(8)}\right)-\frac{\delta_r\varepsilon_r}{R_0}\cos\left(\alpha-\chi-\eta+2\gamma+\varphi+2\psi^{(8)}\right)$$
$$-\beta\frac{\delta_r\varepsilon_z}{R_0}\cos\left(\alpha-\eta+2\left(\gamma+\varphi+\psi^{(8)}\right)\right)-2\beta\varepsilon_z\vartheta\sin\left(\gamma+\varphi+\psi^{(8)}\right)$$
$$-2\delta_r\vartheta\sin\left(\alpha-\eta+\gamma+\varphi+\psi^{(8)}\right) \quad (25a)$$

$$\psi'' = \frac{d^2\psi(0)}{ds^2}=-2\frac{\varepsilon_r}{R_0}\vartheta\cos\left(\chi-\gamma-\psi^{(8)}\right)-2\beta\vartheta\frac{\varepsilon_z}{R_0}\cos\left(\gamma+\varphi+\psi^{(8)}\right)$$
$$-2\frac{\delta_r}{R_0}\vartheta\cos\left(\alpha-\eta+\gamma+\varphi+\psi^{(8)}\right)+\beta\lambda(\sin(\gamma+\varphi)$$

$$
\begin{aligned}
&+\sin\left(\gamma+\varphi+2\psi^{(8)}\right)\Big)-\frac{\varepsilon_r^2}{R_0^2}\sin\left(2\left(\chi-\gamma-\psi^{(8)}\right)\right)\\
&-2\beta\frac{\varepsilon_r\varepsilon_z}{R_0^2}\sin\left(\chi-2\gamma-\varphi-2\psi^{(8)}\right)\\
&+\beta^2\frac{\varepsilon_z^2}{R_0^2}\sin\left(2\left(\gamma+\varphi+\psi^{(8)}\right)\right)+\frac{\beta^2}{2}\sin\left(2\left(\gamma+\varphi+\psi^{(8)}\right)\right)\\
&+\frac{\delta_r^2}{R_0^2}\sin\left(2\left(\alpha-\eta+\gamma+\varphi+\psi^{(8)}\right)\right)+\frac{\lambda^2}{2}\sin\left(2\psi^{(8)}\right)\\
&+2\frac{\varepsilon_r\delta_r}{R_0^2}\sin\left(\alpha-\chi-\eta+2\gamma+\varphi+2\psi^{(8)}\right)\\
&+2\beta\frac{\varepsilon_z\delta_r}{R_0^2}\sin\left(\alpha-\eta+2\left(\gamma+\varphi+\psi^{(8)}\right)\right) \qquad (25b)
\end{aligned}
$$

$$
\begin{aligned}
z'' \;=\; &\frac{d^2z(0)}{ds^2}=-\beta^2\varepsilon_z^2+2\lambda\vartheta R_0\sin\psi^{(8)}\\
&-2\beta\varepsilon_r\cos\left(\chi+\varphi\right)+2\beta\vartheta R_0\sin\left(\gamma+\varphi+\psi^{(8)}\right) \qquad (25c)
\end{aligned}
$$

Introducing (23) into (3), (4) shows that some terms cancel, others double — depending on if they are even or odd with respect to mirror symmetry to the axis $\left(x^{(8)},y^{(8)},z^{(8)}\right)\rightarrow\left(-x^{(8)},-y^{(8)},z^{(8)}\right)$. For instance linear terms in s cancel except for $\psi'\frac{\partial B_z}{\partial\psi}$. The results for h_{13} and h_{24} are lengthy and thus not reported here.

Inserting (12) into these results gives still long expressions with 11 functions characterizing the magnet: b_1, b_2, $\partial b_0/\partial z$, $\partial b_1/\partial z$, $\partial b_2/\partial z$, $\partial b_0/\partial R$, $\partial b_1/\partial R$, $\partial b_2/\partial R$, $\partial^2 b_2/\partial z^2$, $\partial^2 b_2/\partial R^2$, $\partial^2 b_2/\partial R\partial z$. They are reduced to 6 by the 5 substitutions

$$
\begin{aligned}
&\frac{\partial^2 b_2}{\partial R^2}=\frac{-2}{R}\frac{\partial b_1}{\partial z}-\frac{\partial^2 b_2}{\partial z^2},\ \frac{\partial b_1}{\partial R}=\frac{-1}{2}\frac{\partial b_2}{\partial z}-2\frac{b_1}{R},\\
&\frac{\partial b_0}{\partial R}=\frac{-1}{2}\frac{\partial b_2}{\partial z},\quad \frac{\partial b_0}{\partial z}=\frac{b_2}{R}+\frac{\partial b_1}{\partial z},\ \frac{\partial b_2}{\partial R}=\frac{b_2}{R}+2\frac{\partial b_1}{\partial z},
\end{aligned} \qquad (26)
$$

which follow from (15)–(17). The resulting equations for h_{13} and h_{24} are inserted into (22), again all small assembly tolerances are multiplied by the parameter s, and a 2nd order Taylor series in s is computed. This gives the error of an axial angle sensor due to assembly tolerances

$$
\tan\Delta\varphi^{\text{axial}}\cong\tan\Delta\varphi^{\text{axial}}_{\text{min}}+\Lambda^{\text{axial}} \qquad (27)
$$

$$
\begin{aligned}
\tan\Delta\varphi^{\text{axial}}_{\text{min}}=&\frac{3}{4}\beta^2\sin 2\alpha+\frac{3}{4}\lambda^2\sin 2\left(\alpha+\gamma+\varphi\right)\\
&+\beta\lambda\left(\sin\left(\gamma+\varphi\right)+3\sin\alpha\cos\left(\alpha+\gamma+\varphi\right)\right)-\vartheta
\end{aligned} \qquad (28)
$$

$$\begin{aligned}\Lambda^{\text{axial}} = \Lambda_1^{\text{axial}} \frac{b_1\left(R_0, \varepsilon_z + \delta_z\right)}{b_2\left(R_0, \varepsilon_z + \delta_z\right)} + \frac{\Lambda_{1z}^{\text{axial}} R_0}{b_2\left(R_0, \varepsilon_z + \delta_z\right)} \\ \frac{\partial b_1\left(R_0, \varepsilon_z + \delta_z\right)}{\partial z} + \frac{\Lambda_{2z}^{\text{axial}} R_0}{b_2\left(R_0, \varepsilon_z + \delta_z\right)} \frac{\partial b_2\left(R_0, \varepsilon_z + \delta_z\right)}{\partial z} \\ + \Lambda_{2Rz}^{\text{axial}} \frac{R_0^2}{b_2\left(R_0, \varepsilon_z + \delta_z\right)} \frac{\partial^2 b_2\left(R_0, \varepsilon_z + \delta_z\right)}{\partial R \partial z} \\ + \Lambda_{2zz}^{\text{axial}} \frac{R_0^2}{b_2\left(R_0, \varepsilon_z + \delta_z\right)} \frac{\partial^2 b_2\left(R_0, \varepsilon_z + \delta_z\right)}{\partial z^2} \end{aligned} \tag{29}$$

$$\begin{aligned}\Lambda_{2Rz}^{\text{axial}} = (1/(2R_0)) \sin\left(2\left(\alpha + \gamma + \varphi\right)\right) \{\varepsilon_r \lambda \cos\left(\chi - \gamma\right) \\ + \beta\varepsilon_r \cos\left(\chi - 2\gamma - \varphi\right) + \beta\varepsilon_z \lambda \cos\left(\gamma + \varphi\right) + \beta^2 \varepsilon_z \cos\left(2\left(\gamma + \varphi\right)\right) \\ + \delta_r \lambda \cos\left(\alpha - \eta + \gamma + \varphi\right) + \beta\delta_r \cos\left(\alpha - \eta + 2\left(\gamma + \varphi\right)\right)\}\end{aligned} \tag{30a}$$

$$\begin{aligned}\Lambda_{2zz}^{\text{axial}} = (-1/4) \sin\left(2\left(\alpha + \gamma + \varphi\right)\right) \left\{\lambda^2 - \left(\varepsilon_r^2/R_0^2\right) \cos\left(2\left(\chi - \gamma\right)\right)\right. \\ - 2\beta\left(\varepsilon_z \varepsilon_r / R_0^2\right) \cos\left(\chi - 2\gamma - \varphi\right) - \left(\delta_r^2/R_0^2\right) \cos\left(2\left(\alpha - \eta + \gamma + \varphi\right)\right) \\ - 2\left(\delta_r \varepsilon_r / R_0^2\right) \cos\left(\alpha - \chi - \eta + 2\gamma + \varphi\right) + 2\lambda\beta \cos\left(\gamma + \varphi\right) \\ + \beta^2\left(1 - \varepsilon_z^2/R_0^2\right) \cos\left(2\left(\gamma + \varphi\right)\right) \\ \left. - 2\left(\delta_r \beta \varepsilon_z / R_0^2\right) \cos\left(\alpha - \eta + 2\left(\gamma + \varphi\right)\right)\right\}\end{aligned} \tag{30b}$$

$$\begin{aligned}\Lambda_{2z}^{\text{axial}} = (1/R_0)\left(\beta \cos\alpha + \lambda \cos\left(\alpha + \gamma + \varphi\right)\right) \\ \left(\beta\varepsilon_z \sin\alpha + \delta_r \sin\eta + \varepsilon_r \sin\left(\alpha + \chi + \varphi\right)\right)\end{aligned} \tag{30c}$$

$$\begin{aligned}\Lambda_{1z}^{\text{axial}} = \left(3\beta^2/4\right) \sin\left(2\alpha\right) + \beta^2\left(\varepsilon_z^2/R_0^2 + 3/4\right) \sin\left(2\alpha + 4\left(\gamma + \varphi\right)\right) \\ + \left(3\lambda^2/2\right) \sin\left(2\left(\alpha + \gamma + \varphi\right)\right) + \left(\varepsilon_r^2/R_0^2\right) \sin\left(2\left(\alpha - \chi + 2\gamma + \varphi\right)\right) \\ + \left(3\beta\lambda/2\right)\left[\sin\left(2\alpha + \gamma + \varphi\right) + \sin\left(2\alpha + 3\left(\gamma + \varphi\right)\right)\right] \\ + 2\left(\varepsilon_r \beta \varepsilon_z / R_0^2\right) \sin\left(2\alpha - \chi + 4\gamma + 3\varphi\right) \\ + 2\left(\delta_r \varepsilon_r / R_0^2\right) \sin\left(3\alpha - \chi - \eta + 4\gamma + 3\varphi\right) \\ + \left(\delta_r^2/R_0^2\right) \sin\left(4\left(\alpha + \gamma + \varphi\right) - 2\eta\right) \\ + 2\left(\delta_r \beta \varepsilon_z / R_0^2\right) \sin\left(3\alpha - \eta + 4\left(\gamma + \varphi\right)\right)\end{aligned} \tag{30d}$$

$$\begin{aligned}\Lambda_1^{\text{axial}} = (2/R_0) \left\{\beta^2 \varepsilon_z \sin\left(2\alpha + 4\left(\gamma + \varphi\right)\right)\right. \\ + \beta\varepsilon_r \sin\left(2\alpha - \chi + 4\gamma + 3\varphi\right) + \varepsilon_r \lambda \sin\left(2\alpha - \chi + 3\gamma + 2\varphi\right) \\ + \beta\delta_r \sin\left(3\alpha - \eta + 4\left(\gamma + \varphi\right)\right) + \beta\varepsilon_z \lambda \sin\left(2\alpha + 3\left(\gamma + \varphi\right)\right) \\ \left. + \lambda\delta_r \sin\left(3\left(\alpha + \gamma + \varphi\right) - \eta\right)\right\}\end{aligned} \tag{30e}$$

To sum up, the total angle error is composed of two parts:

- The first one is $\Delta\varphi_{\min}^{\text{axial}}$. It depends on the tilt and twist angles of magnet (α, β) and sensor (γ, λ) against the rotation axis, but

it does not depend on the eccentricities $(\varepsilon_r, \delta_r, \chi, \eta)$. It also does not depend on any properties of the magnet.

- The second part of the angle error (Λ^{axial}) is a sum over five derivatives, which account for inhomogeneities of the magnetic field. Therefore they also depend on the radius of the Hall circle (R_0). For one specific magnet numerical values of these derivatives are given in Table A1 of Appendix A.

It is possible to simplify the expression Λ^{axial} for small R_0.

$$\lim_{R\to 0} b_2(R,z) = R \int_{z'=-H/2}^{H/2} \frac{3}{4} R'^2 \frac{z-z'}{\left(R'^2+(z-z')^2\right)^{5/2}}\, dz' \tag{31a}$$

$$\lim_{R\to 0} \frac{1}{R}\frac{\partial b_2(R,z)}{\partial z} = \lim_{R\to 0} \frac{\partial^2 b_2(R,z)}{\partial R \partial z} = \lim_{R\to 0} \frac{-8}{R^2} b_1(R,z)$$
$$= \int_{z'=-H/2}^{H/2} \frac{3}{4} R'^2 \frac{R'^2 - 4(z-z')^2}{\left(R'^2+(z-z')^2\right)^{7/2}}\, dz' \tag{31b}$$

$$\lim_{R\to 0} \frac{1}{R}\frac{\partial^2 b_2(R,z)}{\partial z^2} = \lim_{R\to 0} \frac{-8}{R^2}\frac{\partial b_1(R,z)}{\partial z}$$
$$= \int_{z'=-H/2}^{H/2} \frac{15}{4} R'^2 (z-z') \frac{4(z-z')^2 - 3R'^2}{\left(R'^2+(z-z')^2\right)^{9/2}}\, dz' \tag{31c}$$

Finally one ends up with only two functions that describe the magnet.

$$\lim_{R\to 0} \Lambda^{\text{axial}} = \Lambda_T^{\text{axial}} \tilde{T}^{\text{axial}} + \Lambda_E^{\text{axial}} \tilde{E}^{\text{axial}} \tag{32a}$$

$$\begin{aligned}\Lambda_T^{\text{axial}} = {} & (\beta\cos\alpha + \lambda\cos(\alpha+\gamma+\varphi))(\delta_r \sin\eta + \varepsilon_r \sin(\alpha+\chi+\varphi) \\ & + \beta\varepsilon_z \sin\alpha) + (1/4)\left\{\beta^2\varepsilon_z \sin(2\alpha) + \beta\delta_r \sin(\alpha+\eta)\right. \\ & + \beta\varepsilon_r \sin(2\alpha+\chi+\varphi) + \beta\varepsilon_z\lambda \sin(2\alpha+\gamma+\varphi) \\ & \left. + \delta_r\lambda \sin(\alpha+\eta+\gamma+\varphi) + \varepsilon_r\lambda \sin(2\alpha+\chi+\gamma+2\varphi)\right\}\end{aligned} \tag{32b}$$

$$\begin{aligned}\Lambda_E^{\text{axial}} = {} & (1/8)\left\{\delta_r^2 \sin(2\eta) + \varepsilon_r^2 \sin(2(\alpha+\chi+\varphi)) + \beta^2\varepsilon_z^2 \sin(2\alpha)\right. \\ & + 2\beta\varepsilon_z\delta_r \sin(\alpha+\eta) + 2\beta\varepsilon_z\varepsilon_r \sin(2\alpha+\chi+\varphi) \\ & \left. + 2\delta_r\varepsilon_r \sin(\alpha+\chi+\eta+\varphi)\right\}\end{aligned} \tag{32c}$$

$$\tilde{T}^{\text{axial}} = \lim_{R\to 0} \frac{1}{b_2(R,\varepsilon_z+\delta_z)} \frac{\partial b_2(R,\varepsilon_z+\delta_z)}{\partial z}, \tag{32d}$$

$$\tilde{E}^{\text{axial}} = \lim_{R\to 0} \frac{1}{b_2(R,\varepsilon_z+\delta_z)} \frac{\partial^2 b_2(R,\varepsilon_z+\delta_z)}{\partial z^2} \tag{32e}$$

The so-called shape functions $\tilde{T}^{\text{axial}}$, $\tilde{E}^{\text{axial}}$ are analogous to $\tilde{T}$, $\tilde{E}$ in [1]. They describe how tilts and eccentricities lead to angle errors. Also some of the terms in (32b) and (32c) are identical to (20) in [1]. There is no simple relationship between $\tilde{T}^{\text{axial}}$, $\tilde{T}$ or $\tilde{E}^{\text{axial}}$, $\tilde{E}$.

$$\tilde{T} = \lim_{R\to 0} \frac{1}{R} \frac{b_2\left(R, \varepsilon_z + \delta_z\right)}{b_0\left(R, \varepsilon_z + \delta_z\right)}, \quad \tilde{E} = \lim_{R\to 0} \frac{2}{R^2} \frac{b_1\left(R, \varepsilon_z + \delta_z\right)}{b_0\left(R, \varepsilon_z + \delta_z\right)} \tag{33}$$

Although the shape functions of perpendicular angle sensors were defined as derivatives of field components in [1], they can also be expressed as simple ratios of field components according to (33). Moreover, the relation $\tilde{T}\tilde{T}^{\text{axial}} = -4\tilde{E}$ holds.

4.3. Errors of AxialC8 Sensors due to Assembly Tolerances

An axialC8 sensor is made of two axialC4 sensor layouts rotated against each other by 45°. The rotated axialC4 angle sensor of Fig. 4 has Hall plates at $\left(x^{(8)}, y^{(8)}, z^{(8)}\right) = \left(R_0/\sqrt{2}, R_0/\sqrt{2}, 0\right)$, $\left(-R_0/\sqrt{2}, R_0/\sqrt{2}, 0\right)$, $\left(-R_0/\sqrt{2}, -R_0/\sqrt{2}, 0\right)$, and $\left(R_0/\sqrt{2}, -R_0/\sqrt{2}, 0\right)$. Repeating the calculation of the last subsection gives

$$\tan\Delta\hat{\varphi}^{\text{axial}} \cong \tan\Delta\hat{\varphi}^{\text{axial}}_{\min} + \hat{\Lambda}^{\text{axial}} \tag{34}$$

$$\Delta\varphi^{\text{axial}}_{\min} = \Delta\hat{\varphi}^{\text{axial}}_{\min} \tag{35}$$

$$\begin{aligned}
\hat{\Lambda}^{\text{axial}} = {} & \hat{\Lambda}^{\text{axial}}_1 \frac{b_1\left(R_0, \varepsilon_z + \delta_z\right)}{b_2\left(R_0, \varepsilon_z + \delta_z\right)} + \frac{\hat{\Lambda}^{\text{axial}}_{1z} R_0}{b_2\left(R_0, \varepsilon_z + \delta_z\right)} \frac{\partial b_1\left(R_0, \varepsilon_z + \delta_z\right)}{\partial z} \\
& + \frac{\hat{\Lambda}^{\text{axial}}_{2z} R_0}{b_2\left(R_0, \varepsilon_z + \delta_z\right)} \frac{\partial b_2\left(R_0, \varepsilon_z + \delta_z\right)}{\partial z} \\
& + \hat{\Lambda}^{\text{axial}}_{2R_z} \frac{R_0^2}{b_2\left(R_0, \varepsilon_z + \delta_z\right)} \frac{\partial^2 b_2\left(R_0, \varepsilon_z + \delta_z\right)}{\partial R \partial z} \\
& + \hat{\Lambda}^{\text{axial}}_{2zz} \frac{R_0^2}{b_2\left(R_0, \varepsilon_z + \delta_z\right)} \frac{\partial^2 b_2\left(R_0, \varepsilon_z + \delta_z\right)}{\partial z^2}
\end{aligned} \tag{36}$$

$$\begin{aligned}
\hat{\Lambda}^{\text{axial}}_{2Rz} = {} & \left(1/(2R_0)\right) \cos\left(2\left(\alpha + \gamma + \varphi\right)\right) \left\{\varepsilon_r \lambda \sin\left(\chi - \gamma\right)\right. \\
& + \beta\varepsilon_r \sin(\chi - 2\gamma - \varphi) - \beta\varepsilon_z \lambda \sin(\gamma + \varphi) - \beta^2 \varepsilon_z \sin(2\left(\gamma + \varphi\right)) \\
& \left. - \delta_r \lambda \sin(\alpha - \eta + \gamma + \varphi) - \beta\delta_r \sin(\alpha - \eta + 2\left(\gamma + \varphi\right))\right\}
\end{aligned}$$

$$\begin{aligned}
\hat{\Lambda}^{\text{axial}}_{2zz} = {} & \left(1/4\right) \cos\left(2\left(\alpha + \gamma + \varphi\right)\right) \left\{\left(\varepsilon_r^2/R_0^2\right) \sin\left(2\left(\chi - \gamma\right)\right)\right. \\
& + 2\beta\left(\varepsilon_z\varepsilon_r/R_0^2\right) \sin(\chi - 2\gamma - \varphi) - \left(\delta_r^2/R_0^2\right) \sin(2\left(\alpha - \eta + \gamma + \varphi\right)) \\
& - 2\left(\delta_r\varepsilon_r/R_0^2\right) \sin\left(\alpha - \chi - \eta + 2\gamma + \varphi\right) \\
& + 2\lambda\beta \sin\left(\gamma + \varphi\right) + \beta^2 \left(1 - \varepsilon_z^2/R_0^2\right) \sin\left(2\left(\gamma + \varphi\right)\right) \\
& \left. - 2\left(\delta_r\beta\varepsilon_z/R_0^2\right) \sin\left(\alpha - \eta + 2\left(\gamma + \varphi\right)\right)\right\}
\end{aligned}$$

$$\begin{aligned}
\hat{\Lambda}_{1z}^{\text{axial}} &= \left(3\beta^2/4\right)\sin(2\alpha) - \beta^2\left(\varepsilon_z^2/R_0^2 + 3/4\right)\sin(2\alpha + 4\left(\gamma+\varphi\right)) \\
&\quad - \left(\varepsilon_r^2/R_0^2\right)\sin\left(2\left(\alpha - \chi + 2\gamma + \varphi\right)\right) \\
&\quad + \left(3\beta\lambda/2\right)\left[\sin\left(2\alpha + \gamma + \varphi\right) - \sin\left(2\alpha + 3\left(\gamma + \varphi\right)\right)\right] \\
&\quad - 2\left(\varepsilon_r\beta\varepsilon_z/R_0^2\right)\sin\left(2\alpha - \chi + 4\gamma + 3\varphi\right) \\
&\quad - 2\left(\delta_r\varepsilon_r/R_0^2\right)\sin\left(3\alpha - \chi - \eta + 4\gamma + 3\varphi\right) \\
&\quad - \left(\delta_r^2/R_0^2\right)\sin\left(4\left(\alpha + \gamma + \varphi\right) - 2\eta\right) \\
&\quad - 2\left(\delta_r\beta\varepsilon_z/R_0^2\right)\sin\left(3\alpha - \eta + 4\left(\gamma + \varphi\right)\right) \\
\hat{\Lambda}_1^{\text{axial}} &= -\Lambda_1^{\text{axial}}, \quad \hat{\Lambda}_{2z}^{\text{axial}} = \Lambda_{2z}^{\text{axial}},
\end{aligned} \tag{37}$$

where we denoted the parameters of the 45° rotated system by a hat. For small R the results are identical to the last subsection

$$\lim_{R\to 0}\hat{\Lambda}^{\text{axial}} = \lim_{R\to 0}\Lambda^{\text{axial}} = \Lambda_T^{\text{axial}}\tilde{T}^{\text{axial}} + \Lambda_E^{\text{axial}}\tilde{E}^{\text{axial}} \tag{38}$$

Thus, if an axialC8 sensor estimates the angle by applying some function to the angles $\varphi^{\text{axial}}, \hat{\varphi}^{\text{axial}}$ obtained by the two axialC4 subsystems, its angle error does not change much. In the limit of small R it is even identical to the axialC4 sensor (see (38)). At large R_0 there are differences between (30) and (37), yet they are small.

5. OPTIMUM MAGNET FOR AXIAL ANGLE SENSORS

For arbitrary R it is difficult to find an optimum magnet which minimizes Λ^{axial}. The question is, if a magnet exists, which makes all five derivatives in (29) vanish. It is much simpler to find an optimum magnet for small R, because this only means to make the two shape functions vanish: $\tilde{T}^{\text{axial}} = \tilde{E}^{\text{axial}} = 0$. Since the shape functions of perpendicular and axial angle sensors are different it is obvious that in general optimum magnets are different for both types of sensors.

For a spherical magnet with homogeneous magnetization in y-direction one gets $\tilde{T}^{\text{axial}} = -4/z$, $\tilde{E}^{\text{axial}} = 20/z^2$. This is similar to the shape functions for perpendicular sensors $\tilde{T} = -3/z$, $\tilde{E} = -3/z^2$ [1, 4]. In both cases, the shape functions do not vanish except for large z, which means also large ε_z in Λ_T^{axial}, Λ_E^{axial} so that Λ^{axial} does not vanish.

For cylindrical magnets it is always possible to find an axial position ε_z which makes $\tilde{T}^{\text{axial}}$ vanish: e.g., a 3 mm thick magnet with 10 mm diameter with Hall plates 1.27 mm above or below the magnet. Unfortunately $\tilde{E}^{\text{axial}}$ is large at the zeros of $\tilde{T}^{\text{axial}}$. Therefore the angle error cannot be reduced significantly by this method.

One way to decrease both shape functions is to increase the diameter of a cylindrical sample. This leads to large magnets with

diameters beyond 20 mm. In any case it is preferable to use a large weak magnet (ferrite) instead of a small strong one (rare earth). If both are adjusted to generate the same field strength at the sensor the shape functions of the large magnet are smaller than the ones of the small magnet and this gives smaller errors due to assembly tolerances.

In order to make both shape functions vanish one can use a cylindrical magnet with a small recess in the surface facing the sensor. This strategy worked for the perpendicular angle sensors in [1] and we can also apply it to axial angle sensors. Yet the resulting magnets are different! As an example we assume that the magnet is 3 mm thick, its recess is 1 mm deep, and the sensor should be positioned 2 mm ahead of the recess ($\varepsilon_z = 3.5\,\mathrm{mm}$). The radii of the magnet (R_2') and of the recess (R_1') are two parameters that are varied in order to make the shape functions vanish. The solutions are two curves in

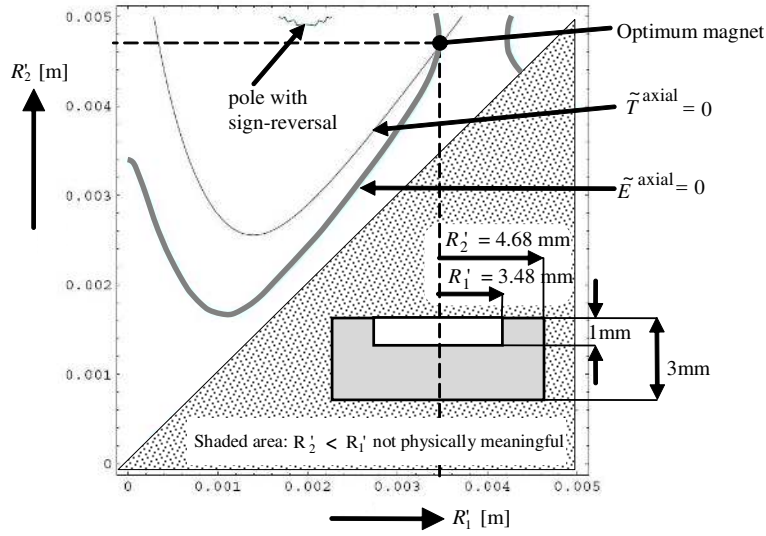

Figure 5. Optimized magnet: Root locus for vanishing shape functions in the (R_1', R_2')-plane. The magnet has a diameter of $2R_2'$ and it is 3 mm thick. It has a 1 mm deep cylindrical hole with diameter $2R_1'$ on its top facing the sensor die. The axial distance between top surface of the magnet and the sensor elements is 2 mm. The magnetization is homogeneous and points in y-direction. At the intersection of the curves both shape functions vanish. Thus the optimum magnet has $R_1' = 3.48\,\mathrm{mm}, R_2' = 4.68\,\mathrm{mm}$ — there the robustness of the angle sensor against assembly tolerances is maximized.

the (R'_1, R'_2)-plane: one curve represents all combinations (R'_1, R'_2) to make $\tilde{T}^{\text{axial}} = 0$, the other curve represents all combinations (R'_1, R'_2) to make $\tilde{E}^{\text{axial}} = 0$. Both curves are given in Fig. 5. Luckily there is an intersection. At this specific set $R'_1 = 3.48\,\text{mm}, R'_2 = 4.68\,\text{mm}$ both shape functions vanish. This gives an optimum magnet with 9.36 mm diameter and 3 mm thickness and a 1 mm deep hole having 6.96 mm diameter.

6. AXIAL VERSUS PERPENDICULAR SENSORS

Although large contributions to the angle error vanish for optimized magnets there is still some part left: $\Delta\varphi_{\text{min}}^{\text{axial}}$ in (28). This is similar to perpendicular angle sensors [1, 4, 5]: also there optimization of magnets can avoid large angle errors but a residual angle error is left

$$\begin{aligned}\tan\Delta\varphi_{\text{min}}^{\text{perpendicular}} &= \left(\beta^2/4\right)\sin 2\alpha + \left(\lambda^2/4\right)\sin 2\left(\alpha+\gamma+\varphi\right) \\ &\quad +\beta\lambda\sin\alpha\cos\left(\alpha+\gamma+\varphi\right) \end{aligned} \tag{39}$$

Comparison of (28) and (39) gives an important relation, which is a central aspect of this work

$$\tan\Delta\varphi_{\text{min}}^{\text{axial}} = 3\tan\Delta\varphi_{\text{min}}^{\text{perpendicular}} + \beta\lambda\sin\left(\gamma+\varphi\right) \tag{40}$$

This means that the angle errors of axial angle sensors are about three times larger than the errors of perpendicular angle sensors.

How can we understand this? In (1) we stated that the ideal magnetic field for axial angle sensors has a z-component which varies linearly against y-position. Yet it also has to satisfy Maxwell's equations, which means that its curl must vanish. Hence the ideal field is

$$\vec{B}^{\text{axial}} = \text{const} \times \left(z\vec{n}_y + y\vec{n}_z\right) \tag{41a}$$

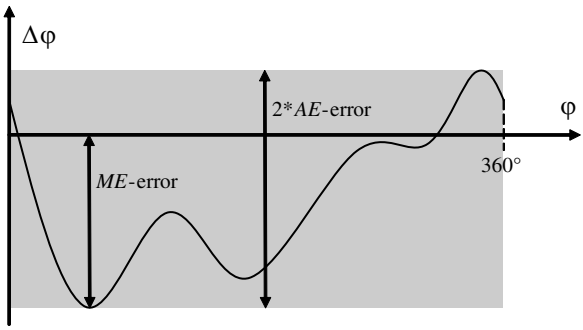

Figure 6. Definition of *ME*-angle error and *AE*-angle error.

This is in contrast to the much simpler homogeneous fields of perpendicular angle sensors

$$\vec{B}^{\text{perpendicular}} = \text{const} \times \vec{n}_y \tag{41b}$$

Perpendicular angle sensors ideally work with homogeneous magnetic fields, whereas axial angle sensors ideally work with fields which are linearly varying in two components. Hence, it is intuitively understandable that homogeneous fields give rise to smaller distortions due to assembly tolerances than inhomogeneous gradient fields.

In order to get a better picture of the difference in errors between axial and perpendicular angle sensors we performed a Monte Carlo simulation with 10000 cases of random assembly tolerances on the basis of (28) and (39) (for optimized magnets). The angles β, λ were Gaussian distributed with zero mean and 1° standard deviation. The angles α, γ were uniformly distributed in [0°, 180°]. ϑ was 0°. For each case the complete curves $\Delta\varphi_{\min}^{\text{perpendicular}}$ and $\Delta\varphi_{\min}^{\text{axial}}$ were computed for the entire revolution $0 < \varphi < 360°$ and the maximum magnitude of $\Delta\varphi_{\min}$ was looked for. This is the *ME*-error as defined in [1, 4, 5]

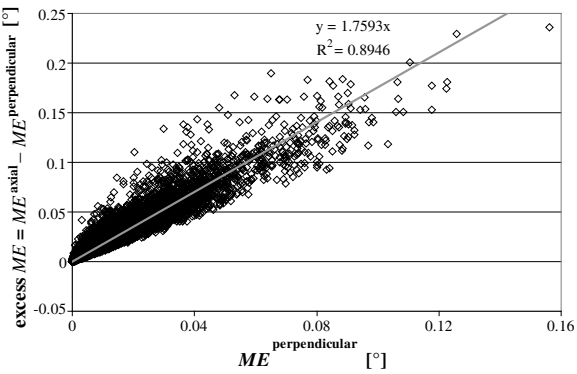

Figure 7. Comparison of *ME*-angle errors for axial and perpendicular systems with optimized magnets. The angle errors are given by (28) and (39). The diagram has 10000 dots, each one representing one case of assembly tolerances of a Monte Carlo simulation. The tilt angles β, λ were Gaussian distributed with zero mean and 1° standard deviation. ϑ was 0°. Under these realistic assumptions the axial angle sensors have roughly 2.8 times larger *ME*-angle errors than perpendicular angle sensors. The excess *ME*-angle error is positive for all 10000 samples — so among the 10000 cases there was not a single case where the axial angle sensor showed smaller error than the perpendicular one.

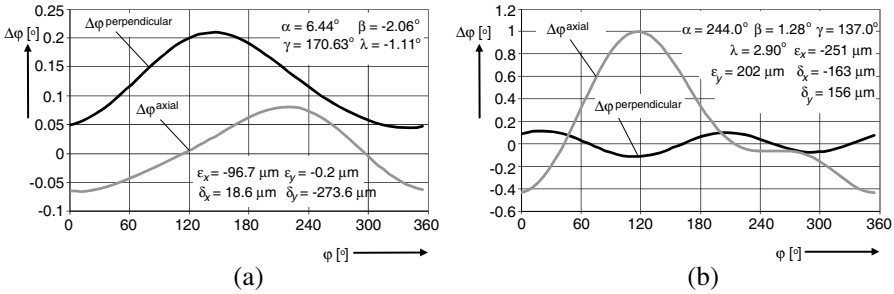

Figure 8. Two specific cases of errors of axial and perpendicular angle sensors from the Monte Carlo simulation of Fig. 9: (a) smallest excess *ME*-error and (b) largest ME-error. The values of assembly tolerances are given in the plots.

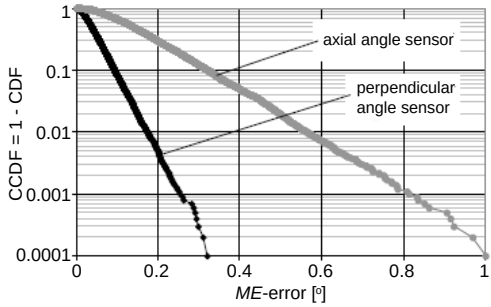

Figure 9. *ME*-angle errors for axial and perpendicular angle sensors with magnet "ML" as defined in [5]. The plot shows the complementary cumulative distribution function (CCDF), which plots the percentage of systems having an *ME*-angle error exceeding the value on the abscissa [4]. This gives $\tilde{T}^{\text{axial}} = -186\,\text{m}^{-1}$, $\tilde{E}^{\text{axial}} = -338938\,\text{m}^{-2}$, $\tilde{T} = 196.1\,\text{m}^{-1}$, $\tilde{E} = 9124.1\,\text{m}^{-2}$. The angle errors are given by (27), (28), (32) for the axial sensor and by (20) in [1]. Both curves in the diagram were obtained by 10000 raw data, respectively, each data point representing one case of assembly tolerances of a Monte Carlo simulation. The angles β, λ were Gaussian distributed with zero mean and 1° standard deviation. ϑ was 0°. The eccentricities ε_x, ε_y, δ_x, δ_y were Gaussian distributed with zero mean and 0.1 mm standard deviation. Angles α, γ were uniformly distributed in [0°, 180°]. Under these realistic assumptions the worst case of 1000 axial angle sensors has 0.8° *ME*-angle error whereas for perpendicular angle sensors it has only 0.25°.

(Fig. 6). It is the largest deviation between estimated and true angle within 360° rotation of the magnet.

The results are shown in Fig. 7, where the excess *ME*-error of axial systems ($= ME^{\text{axial}} - ME^{\text{perpendicular}}$) is plotted on the ordinate and the *ME*-error of perpendicular systems ($= ME^{\text{perpendicular}}$) is plotted on the abscissa. The interesting finding is that for all 10000 cases the excess *ME*-error is positive! This means that in all cases the *ME*-error of axial sensors is larger than the *ME*-error of perpendicular sensors. A linear fit shows that $ME^{\text{axial}} \approx 2.7593 \times ME^{\text{perpendicular}}$. For the same set of data the *AE*-error as defined in [1, 4, 5] and Fig. 6 was also computed. It is half of the difference between maximum and minimum of $\Delta\varphi_{\min}$ in $0° \le \varphi < 360°$. Again the excess *AE*-error of axial systems is positive and a linear fit gives $AE^{\text{axial}} \approx 2.4694 \times AE^{\text{perpendicular}}$. Thus the three results *AE*-error, *ME*-error, and (40) consistently show that axial angle sensors have 2.5, 2.8, and ≈ 3 times larger errors caused by assembly tolerances than perpendicular angle sensors.

In Fig. 7 the *ME*-errors are small: $ME^{\text{perpendicular}} < 0.16°$ and $ME^{\text{axial}} < 0.4°$. This is due to the assumption that the magnets are optimized so that their shape functions vanish. In this paragraph we compare axial and perpendicular sensors for a typical magnet of 10 mm diameter, 2 mm thickness, and a distance of 1 mm between the surface of the magnet and the sensors. The same magnet "ML" was used in [5]. For the perpendicular angle sensors we assumed optimized XMR-layout [1, 5], and for the axial angle sensors we used the small-R approximation (32). As tolerances we assume 1° and 0.1 mm standard

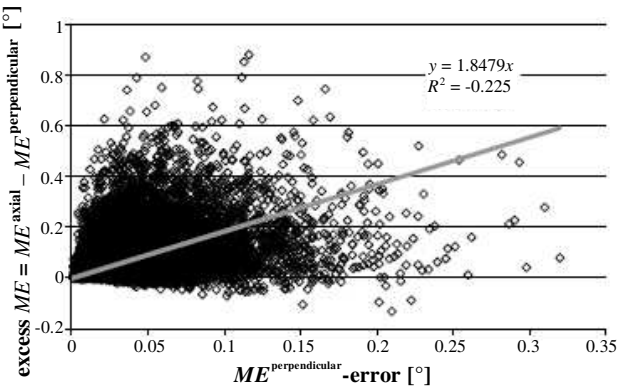

Figure 10. Excess *ME*-errors of axial angle sensors for the data of Fig. 9. It assumes slightly negative values for a few combinations of assembly tolerances, yet the majority of axial angle sensors has larger *ME*-error than perpendicular angle sensors.

deviations and Gaussian distributions with zero mean. The angles α, γ were uniformly distributed in [0°, 180°]. The Monte Carlo simulation comprised 10000 cases of tolerances. Two specific cases are given in Fig. 8. In Fig. 9 the complementary cumulative distribution function CCDF shows a huge difference between axial angle sensor and perpendicular angle sensor: the worst errors of perpendicular systems are nearly 4 times smaller than of axial ones. The data of Fig. 9 is rearranged in Fig. 10, which shows the excess *ME*-error. There it is visible that for some of the 10000 random cases of assembly tolerances the excess *ME*-error is negative (−0.13°). In other words, for these cases the magnet is better suited for axial than for perpendicular angle sensors. Yet on average the perpendicular angle sensor has 2.85 times smaller *ME*-error than the axial angle sensor.

7. CONCLUSION

We coined the terms *axial* versus *perpendicular* angle sensors for angle sensors that estimate the rotational position of a magnet by detecting the magnetic field components *parallel* versus *orthogonal* to the rotation axis. The basic building block of axial angle sensors is the axialC4 cell, where four Hall plates are arranged evenly on a circle that is concentric to the axis of rotation. For good angle accuracy the axialC4 cell needs a diametrically magnetized magnet of rotational symmetry (Fig. 3). Contrarily perpendicular angle sensors work with all shapes of magnets. The axial angle sensor can make up for this insufficiency by adding a second axialC4 cell, the layout of which is rotated against the first axialC4 cell by 45°. In such an axialC8 sensor both subsystems estimate the rotation angle and the system uses the average of both estimations as best guess (Fig. 4).

The dominant part of angle errors is caused by assembly tolerances of magnet and sensor versus rotation axis (tilts and eccentricities). Assembly tolerances lead to distortions of the field on the sensor. Due to the nonlinearity of these distortions the error caused by several simultaneous tolerances is notably larger than the sum of errors of individual tolerances [5]. Therefore the worst case out of thousand systems in the production line has a significantly larger angle error than typical systems (Fig. 9). For axial sensors the errors caused by assembly tolerances are minimized by optimized magnets with vanishing shape functions (Fig. 5). Also the error of perpendicular angle sensors can be minimized by optimized magnets, yet the magnets for axial and perpendicular sensors are different.

Even for optimized shapes of the magnet a certain angle error is unavoidable due to assembly tolerances, namely tilts of magnet and

sensor against the rotation axis. This holds for all kinds of magnetic angle sensors. However, for axial angle sensors this unavoidable angle error is three times larger than for perpendicular angle sensors (see (40)). These differences are not just theoretical — they are indeed relevant in practice, particularly in high volume production. In the future it should be possible to reduce these errors by adding a soft magnetic layer with high permeability across the entire bottom surface of the sensor die according to [16].

APPENDIX A.

In Table A1 we summarize the magnetic field derivates of (29) for the magnet of Fig. A1.

APPENDIX B.

Here we discuss the angle error caused by the magnetic nonlinearity of the Hall plates. Thereby we neglect assembly tolerances. At large

Table A1. Magnetic field derivatives for the magnet of Fig. A1 at $R_0 = 1\,\text{mm}$. b_0, b_1, b_2 were checked by a finite element simulation.

z [mm]	b_0	b_2	$\frac{b_1}{b_2}$
−2.5	−0.110	−0.023	0.019
2.5	−0.099	0.020	−0.002
$\frac{R}{b_2}\frac{\partial b_1}{\partial z}$	$\frac{R}{b_2}\frac{\partial b_2}{\partial z}$	$\frac{R^2}{b_2}\frac{\partial^2 b_2}{\partial z^2}$	$\frac{R^2}{b_2}\frac{\partial^2 b_2}{\partial R \partial z}$
0.046	−0.150	−0.382	−0.122
0.022	0.012	−0.176	−0.011

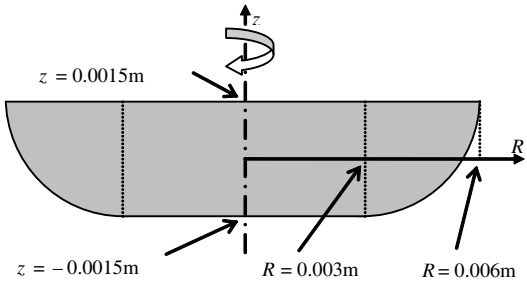

Figure A1. Magnet with rotational symmetry. The magnetization is homogeneous and points in y-direction.

fields the Hall signal is proportional to

$$h \propto B_z / \left(1 - (8/\pi - 1)\, \mu^2 B^2\right) \tag{B1}$$

with the Hall mobility $\mu \approx 0.14/\mathrm{T}$ in silicon and $B^2 = B_x^2 + B_y^2 + B_z^2$ [17]. The question is if the denominator may lead to angle errors. For magnets with homogeneous magnetization in y-direction and rotational shape Section 3.2 gives

$$B^2 = (\mu_0 M)^2 \left\{ b_0^2 + b_1^2 + b_2^2/2 - \cos(2\varphi) \left(2 b_0 b_1 + b_2^2/2\right) \right\} \tag{B2}$$

So if the magnet fulfils the condition

$$-4 b_0 b_1 = b_2^2 \tag{B3}$$

the magnetic nonlinearity of the Hall plates leads to zero angle error. The task is to find values for $\varepsilon_z, H, R'(z')$ that fulfil (B3) for a given R (which is determined by the layout of the sensor).

Inserting (B1) and (B2) into (28) with $\alpha = \gamma = 0$ gives the angle error caused by the nonlinearity of the Hall effect

$$\Delta\varphi_{NL} \cong (8/\pi - 1) \left(\mu \mu_0 M\right)^2 \left(b_0 b_1 + b_2^2/4\right) \sin(4\varphi) \tag{B4}$$

With the values of Table A1 we obtain small errors: $0.00018°$ at $z = -0.0025\,\mathrm{m}$ and $0.00032°$ at $z = -0.0025\,\mathrm{m}$ for $\mu_0 M = 1\,\mathrm{T}$. Moreover the argument from Section 3.2 again holds: since the error has a $90°$ periodicity it is greatly reduced in an axialC8 system. Thus the nonlinearity of the Hall effect in silicon does not play a notable role in errors of axial angle sensors.

APPENDIX C.

So far we assumed that the chip surface is exactly plain. Yet, in [18] it was proven that the chip has a typical warpage of about $0.1°$ depending on temperature, aging of organic materials, and moisture content of the mould compound of the sensor package. Axial sensors are larger than perpendicular ones due to the Hall circle with diameter $2R_0$. Does this warpage lead to angle errors?

We assume a test point at azimuthal position $\psi = \varphi$ in Fig. C1. When the magnet is rotated by φ in negative direction this point is at Hall plate 1. There the axial field component is $B_z(\varphi)$ and the radial one is $B_R(\varphi) = B_x(\varphi)\cos\varphi + B_y(\varphi)\sin\varphi$. The normal field on the Hall plate 1 is

$$B_1^{\perp} = B_z(\varphi)\cos\theta + B_R(\varphi)\sin\theta \tag{C1}$$

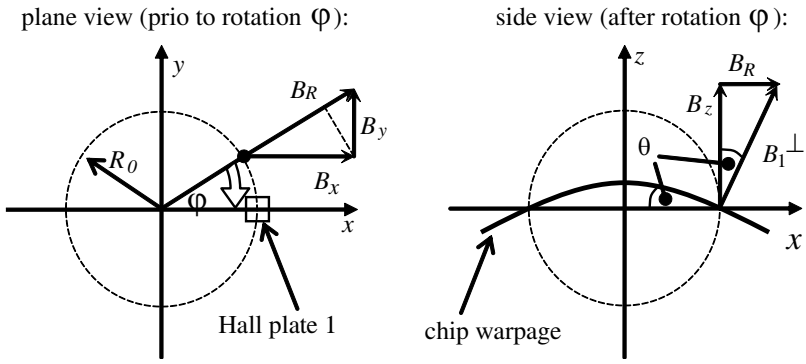

Figure C1. Magnetic field components on a warped chip.

For the other Hall plates we have to replace $\varphi \to \varphi + \psi^{(8)}$. With (12a)–(12c) we get the signals

$$h_{13} = 2\,(b_2 \cos\theta + (b_0 + b_1)\sin\theta)\sin\varphi \tag{C2}$$

$$h_{24} = 2\,(b_2 \cos\theta + (b_0 + b_1)\sin\theta)\cos\varphi \tag{C3}$$

Symmetric warpage across x- and y-axis of the chip would not lead to errors. Yet asymmetric warpage means $\theta = \theta_y$ in (C2) and $\theta = \theta_x$ in (C3) with $\theta_x \neq \theta_y$. This leads to an angle error

$$\sin\Delta\varphi_{\text{warp}} = \frac{h_{13}\cos\varphi - h_{24}\sin\varphi}{\sqrt{h_{13}^2 + h_{24}^2}} \cong \frac{\sin(2\varphi)}{2\sqrt{2}}\frac{b_0 + b_1}{b_2}(\theta_y - \theta_x) \tag{C4}$$

Inserting the numbers of Table A1 for the magnet of Fig. A1 gives $\Delta\varphi_{\text{warp}} \cong 1.7(\theta_y - \theta_x)\sin(2\varphi)$. For the warpage we take the measured values of Fig. 19 in [18]: at low temperature we get $\theta_x = 0.076°$, $\theta_y = 0.05°$ for $2R = 1.1\,\text{mm}$. This leads to an angle error of $0.044°$. Note that even though the warpage (in Fig. 19 in [18]) is smaller at room temperature the difference $\theta_y - \theta_x$ is constant up to 70°C.

To sum up: warpage is not a significant problem as long as the Hall circle has a diameter about 1 mm and the aspect ratio of chip and package is within $0.7 \ldots 1.4$.

APPENDIX D.

This paper discussed axial angle sensors that estimate the angular position of the magnet by the gradient of the plane $B_z\left(x^{(8)}, y^{(8)}, z^{(8)} = 0\right)$, which leads to (21). The state of the art knows different algorithms which look for the zero crossing of the field $B_z(x^{(8)}, y^{(8)}, z^{(8)} = 0) = 0$.

To this end they place an array of Hall plates on the die and look for neighbors detecting magnetic fields with opposite polarity. Since the field has a $\sin\psi$-behavior one can interpolate the exact ψ-value for zero-crossing between these two neighbors. This algorithm is simpler than the arctan-calculation in (21), which saves resources and time delay. It is also better than axialC4 systems because it works with general shapes of magnets just like axialC8 systems. Yet, it does not reduce angle errors caused by assembly tolerances, because they result from the distortion of the field onto the tilted chip surface. The problem of mismatch of Hall plates is slightly less, because the neighboring Hall plates are closer than the Hall plates in an axialC4 angle sensor, which usually improves matching. However, simple zero tracking systems do not cancel homogeneous disturbance fields any more: a background field lifts the entire B_z-plane thereby shifting the zero trace laterally so that it does not go through the rotation axis any more. Better algorithms detect also the second neighbor pair of Hall plates around the zero-crossing which is roughly opposite the first one. Then it is again possible to cancel homogeneous disturbance fields.

All algorithms fit a plane into an array of test points defined by the Hall plates on the chip. They compute the orientation of this plane (which correlates with the zero crossing of this plane) and infer the rotation angle. The details of signal conditioning differ between various types of axial angle sensors, but the results of Sections 4, 5, 6 still hold.

APPENDIX E.

Mechanical stress affects offset and magnetic sensitivity of Hall plates. We briefly discuss its influence on the angle error.

If the Hall plates are operated in a spinning current scheme [12], the raw offset of about 10 mT is reduced by two to three orders in magnitude so that finally the signals only have a residual offset of about 30 µT. If the B_z-field is 30 mT at each Hall plate the signals are

$$h_{13} = 2 \times 30\,\mathrm{mT} \times \sin\varphi \pm \sqrt{2} \times 30\mu\mathrm{T}, \tag{E1a}$$

$$h_{24} = 2 \times 30\,\mathrm{mT} \times \cos\varphi \pm \sqrt{2} \times 3\breve{0}\mu\mathrm{T} \tag{E1b}$$

Thereby the 30 µT of h_{13} and the $3\breve{0}$ µT of h_{24} are uncorrelated, because they originate from different pairs of Hall plates. With (22) the error caused by offset at rotational position φ is

$$\tan\Delta\varphi_{\mathrm{off}} = \frac{\begin{array}{c}\left(2 \times 30\,\mathrm{mT} \times \cos\varphi \pm \sqrt{2} \times 3\breve{0}\mu\mathrm{T}\right)\sin\varphi \\ -\left(2 \times 30\,\mathrm{mT} \times \sin\varphi \pm \sqrt{2} \times 30\mu\mathrm{T}\right)\cos\varphi\end{array}}{2 \times 30\,\mathrm{mT} + \sqrt{2}\left(\pm 30\mu\mathrm{T} \pm 3\breve{0}\mu\mathrm{T}\right)\sin\varphi\cos\varphi} \tag{E2}$$

The worst case angle error occurs at $\varphi = 45°$. It is

$$\Delta\varphi_{\text{off}} < \arctan \frac{\sqrt{2} \times 30\mu\text{T}}{2 \times 30\,\text{mT}} = 0.04° \tag{E3}$$

Hence, with strong magnets the offset does not give large errors.

The magnetic sensitivity of Hall plates depends on the sum of in-plane stress components $\propto (1 + P_{12}(\sigma_{xx} + \sigma_{yy}))$, with $P_{12} \approx 45\%/\text{GPa}$ [14]. The current which supplies the Hall plates is defined by resistors, which suffer from piezo-resistivity of about $-24\%/\text{GPa}$ in the case of generally used n-doped resistors [14]. Thus the Hall output signals have a sensitivity to mechanical stress of roughly $69\%/\text{GPa}$. If all Hall plates experience the same mechanical stress this would not affect the angle error, because equal factors in the nominator and denominator of (22) cancel. However, in practice the package is not symmetrical and the die is positioned asymmetrically due to pick-and-place tolerances at the assembly line. SMD packages suffer from mechanical stress asymmetries coupled from printed circuit boards to the chip. For a guess of inhomogeneities of mechanical stress on the Hall plates we refer to [18]: there measurements in Fig. 20 show that $\sigma_{xx}+\sigma_{yy}$ changes by 80 MPa between packages that were first dried out in an oven and afterwards stored at large ambient humidity for several days. We estimate that stress inhomogeneity across the Hall circle is equal to at least 1/8th of this stress drift. This gives a mismatch of $69\%/\text{GPa} \times 10\text{MPa} = 0.69\%$ between h_{13} and h_{24}. With (22) the error is

$$\tan\Delta\varphi_{\text{mismatch}} = \frac{\cos\varphi\sin\varphi - (1-0.0069)\sin\varphi\cos\varphi}{\cos^2\varphi + (1-0.0069)\sin^2\varphi} \tag{E4}$$

So the worst case angle error is

$$\Delta\varphi_{\text{mismatch}} < \arctan(0.0069/2) = 0.2° \tag{E5}$$

Thus, stress induced mismatch is a significant source of errors in axial angle sensors. Note that stress is not constant versus lifetime; it depends on temperature and moisture content of the mold compound of the sensor package and the printed circuit board. One efficient way to tackle this problem is by way of stress compensation circuits [19, 20].

With (E5) we can also take account of other sources of mismatch in magnetic sensitivity of the Hall plates (e.g., spread of thickness of Hall plate) by replacing the factor 0.0069 with the mismatch.

REFERENCES

1. Ausserlechner, U., "Inaccuracies of anisotropic magneto-resistance angle sensors due to assembly tolerances," *Progress In Electromagnetics Research B*, Vol. 40, 79–99, 2012.

2. Granig, W., St. Hartmann, and B. Köppl, "Performance and technology comparison of GMR versus commonly used angle sensor principles for automotive applications," *SAE World Congress & Exhibition*, SAE document No. 2007-01-0397, Detroit, USA, Apr. 2007.
3. Granig, W., J. Zimmer, Ch. Kolle, D. Hammerschmidt, B. Schaffer, R Borgschulze, and Ch. Reidl, "Integrated giant magnetic resistance based angle sensor," *Proc. IEEE Sensors*, 542–545, Daegu, Korea, Oct. 2006.
4. Ausserlechner, U., "Inaccuracies of giant magneto-resistive angle sensors due to assembly tolerances," *IEEE Trans. Magn.*, Vol. 45, No. 5, 2165–2174, May 2009.
5. Ausserlechner, U., "The optimum layout for giant magneto-resistive angle sensors," *IEEE Sens. J.*, Vol. 10, No. 10, 1571–1582, 2010.
6. Demierre, M., E. Schurig, Ch. Schott, P. A. Besse, and R. S. Popovic, "Contactless 360° absolute angular CMOS microsystem based on vertical hall sensors," *Sensors and Actuators*, Vol. A116, 39–44, 2004.
7. Pascal, J., L. Hebrard, and V. Frick, "3D Hall probe integrated in 0.35 µm CMOS technology for magnetic field pulses measurements," *Circuits and Systems and TAISA Conf. 2008, NEWCASTAISA 2008*, 97–100, Conf. Publications, 2008.
8. Reymond, S., P. Kejik, and R. S. Popovic, "True 2D CMOS integrated hall sensor," *IEEE Sensors Conf.*, 860–863, 2007.
9. Metz, M., A. Häberli, M. Schneider, R. Steiner, C. Maier, and H. Baltes, "Contactless angle measurement using four hall devices on single chip," *Transducers'97 Int'l Conf Solid-State Sensors and Actuators*, 385–388, Chicago, Jun. 16–19, 1997.
10. Gao, X. H., M. H. Jin, L. Jiang, Z. W. Xie, P. He, L. Yang, Y. W. Liu, R. Wei, H. G. Cai, H. Liu, J. Butterfass, M. Grebenstein, N. Seitz, and G. Hirzinger, "The HIT/DLR dexterous hand: Work in progress," *Proc. IEEE Int'l Conf Robotics & Automation*, 3164–3168, Taipei, Taiwan, Sep. 14–19, 2003.
11. Takahashi, T., Y. Nagano, and S. Kawahito, "Development of a high precision angle sensor," *NTN Techn. Rev.*, No. 73, 98–103, 2005.
12. Ausserlechner, U., "Limits of offset cancellation by the principle of spinning current Hall probe," *Proc. IEEE Sensors*, Vol. 3, 1117–1120, 2004.

13. Ausserlechner, U., M. Motz, and M. Holliber, "Compensation of the piezo-Hall effect in integrated Hall sensors on (100)-Si," *IEEE Sens. J.*, Vol. 7., No. 11, 1475–1482, 2007.
14. Ausserlechner, U., M. Motz, and M. Holliber, "Drift of magnetic sensitivity of smart Hall sensors due to moisture absorbed by the IC-package," *Proc. IEEE Sensors*, Vol. 1, 455–458, 2004.
15. Engel-Herbert, R. and T. Hesjedal, "Calculation of the magnetic stray field of a uniaxial magnetic domain," *J. Appl. Phys.*, Vol. 97, 074504, 4pages, 2005.
16. Ausserlechner, U., "Integrierter differentieller magnetfeldsensor," Patent DE10314602, Mar. 31, 2003.
17. Seeger, K., *Semiconductor Physics*, Springer Series in Solid-State Sciences 40, 4th Edition, Eq. (4.2.35) at p. 56, Springer, Berlin, 1988.
18. Husstedt, H., U. Ausserlechner, and M. Kaltenbacher, "In-situ analysis of deformation and mechanical stress of packaged silicon dies with an array of Hall plates," *IEEE Sens. J.*, Vol. 11, No. 11, 2993–3000, 2011.
19. Ausserlechner, U., "Concept for compensating the influences of external disturbing quantities on physical functional parameters of integrated circuits," Patent US6906514, Jun. 14, 2005.
20. Ausserlechner, U., "Magnetic field sensor apparatus," Patent US7474093, Jan. 6, 2009.